Inorganic Chemistry
Article
Cite This: *Inorg. Chem.* XXXX, XXX, XXX−XXX
pubs.acs.org/IC

Hollow Polyhedral Arrays Composed of a Co_3O_4 Nanocrystal Ensemble on a Honeycomb-like Carbon Hybrid for Boosting Highly Active and Stable Evolution Oxygen

Xuan Kuang,*,† Rui Kuang,*,‡ Yanfang Dong,† Zhiling Wang,† Xu Sun,† Yong Zhang,† and Qin Wei*,†

†Key Laboratory of Interfacial Reaction & Sensing Analysis in Universities of Shandong, Shandong Provincial Key Laboratory of Fluorine Chemistry and Chemical Materials, School of Chemistry and Chemical Engineering, University of Jinan, Jinan 250022, China

‡College of Traffic Civil Engineering, Shandong Jiaotong University, Jinan 250023, China

Supporting Information

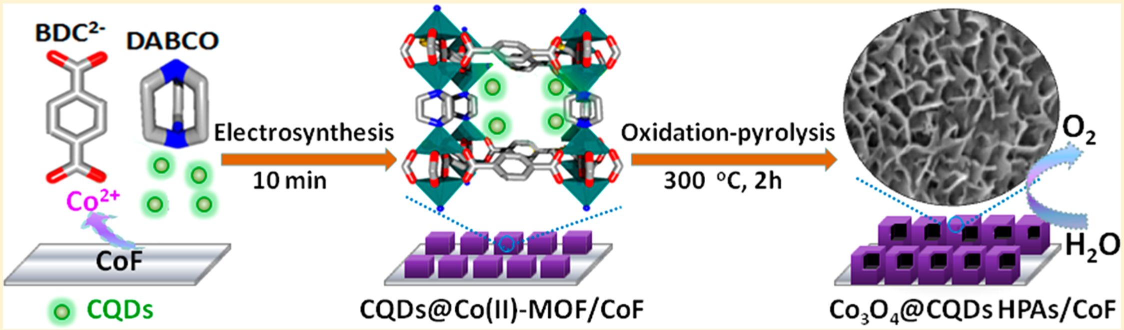

ABSTRACT: We synthesize hollow polyhedral arrays composed of honeycomb-like nanosheets of Co_3O_4 nanocrystals imbedded on carbon quantum dots (CQDs)- and nitrogen-codoped carbon matrix via a facile in situ air oxidation pyrolysis for CQDs-incorporated metal−organic framework polyhedral arrays. The function of CQDs hollowing and forming porous nanosheet shells was found. The resulting hierarchical architecture displays excellent oxygen evolution reaction activity with a low overpotential of 301 mV to drive 100 mA cm^{-2} in 1.0 M KOH and long-playing durability in oxygen evolution. The high performance can be ascribed to its highly dispersed Co_3O_4 nanocrystals, CQDs and nitrogen codoping, internal cavities, and hierarchical pore system.

1. INTRODUCTION

Driven by the ever-growing demand for a clean and highly efficient hydrogen energy source, many more research efforts focus on the rational design and preparation of highly efficient, stable, and cost-efficient oxygen evolution reaction (OER) electrocatalysts because of their sluggish kinetic barrier, thus leading to a high overpotential as the energy-intensive step.[1−4] Spinel Co_3O_4 is a promising candidate to replace scarce noble-metal catalysts like IrO_2 or RuO_2 because of its natural abundance and proper redox capability in alkaline media.[5] To overcome the inherent deficiency of a single material, it is very meaningful for engineering complex Co_3O_4 micro/nanostructures to (i) expose intrinsic catalytic sites, (ii) enhance the electroconductivity, (iii) chance the mass-transfer properties, and (iv) increase the limited electrode surface area.[4]

As a unique architecture, hollow micro/nanostructures with well-defined internal cavities, functional shell components are more attractive electrocatalysts in the OER process because of their more electrochemical active sites and shortened pathways for gas and electrolyte diffusion and thus facilitated charge/mass transport and catalytic kinetics over solid counterparts.[6,7] However, the compact shells lead to the inner part being inactive because of the greatly hampered inward diffusion. Therefore, hollow Co_3O_4 micro/nanostructures with permeable porous thin shells are highly desired for the OER process.[8] Further, Co_3O_4 nanocrystals imbedded on hollow porous supports, which can disperse and protect the catalysts from leach-out and/or aggregation, are the optimized alternatives.

Carbon materials have been demonstrated to be ideal candidates for supporting various nanocatalysts because of their high surface areas, controllable morphologies, and outstanding chemical and thermal stability.[9] Doping of functional heteroatoms (such as nitrogen) into carbon networks can effectively tune their intrinsic electronic structures because of their higher electronegativity (3.04) relative to carbon (2.55) and thus improve their catalysis activity.[10,11] Despite this, various contemporary carbon

Received: November 24, 2018

DOI: 10.1021/acs.inorgchem.8b03236
Inorg. Chem. XXXX, XXX, XXX−XXX

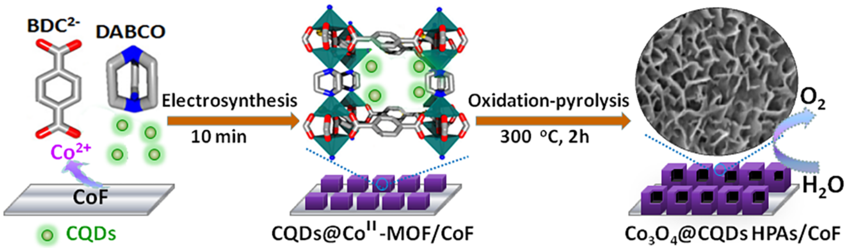

Figure 1. Schematic illustration to form Co_3O_4@CQDs-CN HPAs/CoF.

materials such as multiwalled carbon nanotubes and graphenes have been applied to obtain the required morphologies and compositions.[12] For the fabrication of hollow polyhedral structures, the materials do not apply because of the restriction of their morphologies. A traditional hard-template approach is known as the most efficient route but suffers from complicated conditions such as time- and energy-consuming problems for template removal.[13] The soft-template approach, like surfactants and organic polymers, is also limited because this generates the nanoparticles (NPs) of nonuniform distribution in hollow structures.[14] For these, novel and facile strategies, especially the engineering of self-supported hollow porous polyhedral nanoarrays as binder-free electrodes that (i) allow for straightforward template removal and (ii) create a functional matrix of dispersing Co_3O_4 nanocrystals to maximize their surface areas, catalytic active sites, and catalytic stability, represent alternative ways to accelerate the OER,[1,10,15] which, however, have been not reported.

Herein, we report the novel hollow polyhedral arrays grown on Co foil (CoF), where polyhedra are composed of porous honeycomb-like nanosheet arrays of Co_3O_4 nanocrystals imbedded on a carbon quantum dots (CQDs)- and nitrogen-codoped carbon matrix (denoted as Co_3O_4@CQDs-CN HPAs/CoF). The hierarchical architecture is derived from a facile in situ air oxidation pyrolysis for CQDs-incorporated cobalt-based metal−organic framework polyhedral arrays (denoted as CQDs@Co^{II}-MOF/CoF) at 300 °C. The present Co^{II}-MOF, $Co_2(1,4\text{-BDC})_2(DABCO)\cdot 4DMF\cdot H_2O$ (DMF = *N*,*N*′-dimethylformamide), was employed because of its porous well-defined 3D crystalline framework constructed from Co^{II} cations and organic linkers nitrogen-rich 1,4-diazabicyclo[2.2.2]octane (DABCO) and aromatic 1,4-benzenedicarboxylic acid (H_2BDC) at the molecular level. By oxidation pyrolysis, the structure-controlling template is expected to transform into a porous polyhedron where cobalt oxide NPs are embedded in a nitrogen-doped carbon matrix. Further, it will be more promising that the MOF precursor is loaded into noninnocent guest molecules in framework pores by host−guest chemistries, which may generate the hierarchical structure with novel functionalities under pyrolysis, although thus far few researches are reported in this strategy.[16−18] The unique organic−inorganic constitutes enable MOFs to be especially suitable as precursors for widespread carbon nanomaterials.[19] CQDs were utilized for their small and narrow size distribution (<10 nm) and abundant surface functional groups (e.g., $-NH_2$, $-COOH$, and $-OH$) that enable strong interaction (e.g., hydrogen bonding) with MOFs[20,21] and would endow novel functionality to the resulting hybrid. Surprisingly, CQDs have a hollowing function and involved oxidation, accounting for the shell formation of porous nanosheet arrays. Also, Co_3O_4@CQDs-CN HPAs/CoF display remarkable improved OER activity and long-term durability. The low overpotential of 301 mV to attain 100 mA cm^{-2} in 1.0 M KOH precedes a series of benchmarking Co_3O_4-based OER electrocatalysts in alkaline media (Table S1). To the best of our knowledge, this is the first hybrid by CQDs hollowing, which offers a new strategy for enhancing the electrocatalytic performance.

2. EXPERIMENTAL SECTION

2.1. Synthesis of CQDs. CQDs were easily and quickly prepared using microwave irradiation. Briefly, an aqueous solution of the carbon precursor D-glucose (1.67 mmol, 0.3 g) and NaH_2PO_4 (0.72 mmol, 0.1 g) acted as the foaming agent to accelerate the reaction, and ultrapure water (2 mL) in a 350 W domestic microwave oven was heated for 1.5 min. Thus, a brown-yellow colloidal solid was obtained. The colloidal solid was dispersed in deionized water, centrifuged at 12000 rpm for 30 min to remove the large particles, and then dried by microwave at a low power of 250 W. Thus, 56 mg of CQDs was obtained.

2.2. Preparation of Co_3O_4@CQDs-CN HPAs/CoF and Co_3O_4@CN/CoF. Typically, Co_3O_4@CQDs-CN HPAs/CoF was synthesized via a facile yet simple two-step process. Typically, CoF was first treated with diluted hydrochloric acid (1.0 M HCl) and then washed with ethanol and water several times. DABCO (1.0 mmoL) and H_2BDC (1.0 mmoL) were added to a mixed solvent of ethanol (1 mL) and DMF (4 mL). Then, a LiOH aqueous solution (1 mL, 3.7%) was slowly dropped into the mixture to form a transparent ligand solution. The CQDs (56 mg) were also dispersed in the ligand solution, where the CQDs concentration was 11.2 mg mL^{-1}. CQDs@Co^{II}-MOF were directly grown on conductive CoF in the ligand solution. A standard three-electrode system was used with a CoF (1 cm × 1 cm) as the working electrode and a Pt wire and Hg/HgO as the counter and reference electrodes, respectively. CQDs@Co^{II}-MOF/CoF was obtained by applying a constant oxidation potential (+1.5 V) for the solution for 10 min at 15 °C.

For comparison, Co^{II}-MOF/CoF was also prepared using the same preparation process as that of CQDs@Co^{II}-MOF/CoF, except that a recipe without CQDs was involved.

The as-prepared CQDs@Co^{II}-MOF/CoF and Co^{II}-MOF/CoF were heated to 300 °C with a heating rate of 5 °C min^{-1} and kept for 2 h in a tube furnace under air. After the tube furnace was cooled to room temperature at a rate of 2 °C min^{-1}, the products Co_3O_4@CQDs-CN HPAs/CoF and Co_3O_4@CN/CoF were harvested.

2.3. Preparation of Ru_2O/CoF. Powdered RuO_2 was prepared according to a previous report.[16] Next, 3.4 mg of RuO_2 powder was dispersed in the solvents composed of 720 μL of water, 250 μL of ethanol, and 30 μL of a Nafion solution (5 wt %), followed by ultrasonication for 15 min. Then, 100 μL of a homogeneous RuO_2 suspension was coated onto the 1 cm^2 CoF, followed by drying at 50 °C. The procedure was repeated five times (RuO_2 loading: 1.7 mg cm^{-2}).

3. RESULTS AND DISCUSSION

Co_3O_4@CQDs-CN HPAs/CoF, as shown in Figure 1, was synthesized via a facile yet simple two-step process: electrodeposition for the synthesis of CQDs@Co^{II}-MOF/CoF and oxidation pyrolysis for the final product. First, the CQDs@

DOI: 10.1021/acs.inorgchem.8b03236
Inorg. Chem. XXXX, XXX, XXX−XXX

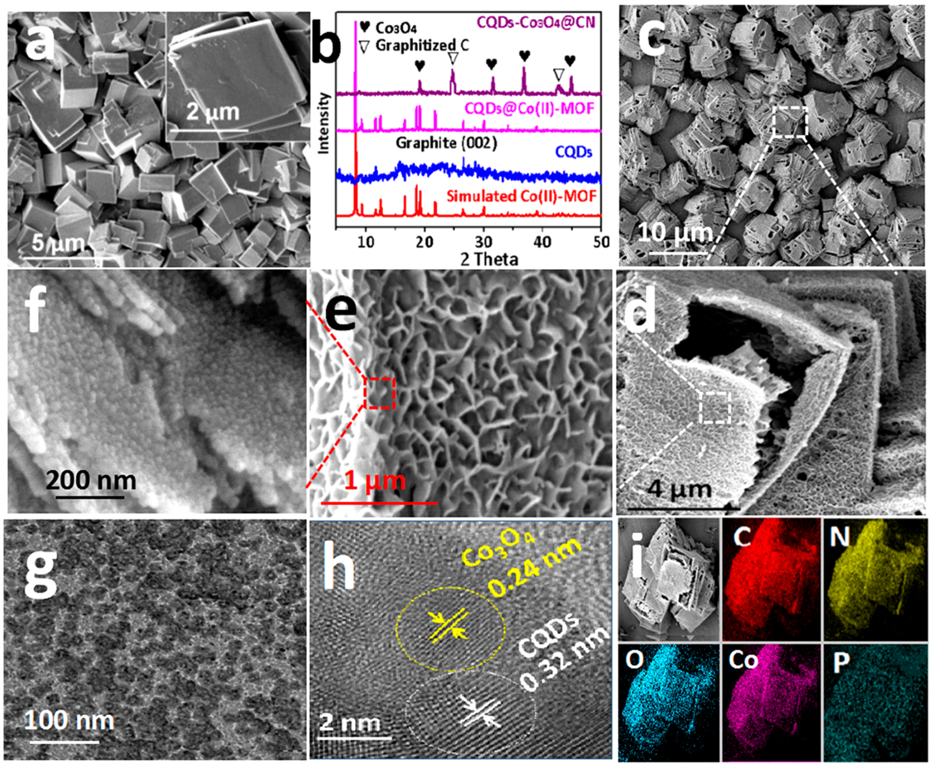

Figure 2. (a) FE-SEM images of CQDs@Co^{II}-MOF (inset: its high-magnifcation FE-SEM image). (b) XRD patterns of CQDs, CQDs@Co^{II}-MOF, and Co_3O_4@CQDs-CN HPAs (c−e) FE-SEM images. (g) TEM and (h) high-magnification TEM images. (i) SEM−EDS elemental mapping of Co_3O_4@CQDs-CN HPAs.

Co^{II}-MOF was directly grown on conductive CoF by a potentiostatic oxidation in a solution of CQDs and the mixed ligands DABCO and H_2BDC. A CoF used as the working electrode was oxidized, and released Co^{II} ions coordinated to the ligands to fabricate CQDs@Co^{II}-MOF/CoF. The field-emission scanning electron microscopy (FE-SEM) images clearly reveal that the CQDs@Co^{II}-MOF as a well-defined tetrahedron covers the CoF (Figure 2a). A close-up inspection (inset of Figure 2a) finds that the tetrahedron consists of multiple, closely packed lamellae with smooth surfaces, the edge dimensions of which range from ~2 to 3 μm. The X-ray diffraction (XRD) pattern of CQDs@Co^{II}-MOF matches with the simulated pattern of $Co_2(1,4\text{-}BDC)_2(DABCO)\cdot 4DMF\cdot H_2O$ (Figure 2b),[22] indicating the same crystalline structures. The photoluminescence (PL) spectrum of CQDs@Co^{II}-MOF powders shows an obvious emission peak of CQDs at ~365 nm excited at 295 nm (Figures S1 and S2). An evident blue shift from that of CQDs suggests that Co^{II}-MOF can fix CQDs and block the aggregation of CQDs.[23] However, the diffraction pattern of CQDs with the lattice planes of graphitic carbon[24] does not appear in the XRD pattern of CQDs@Co^{II}-MOF (Figure 2b). From these, we can conclude that CQDs are incorporated into the Co^{II}-MOF pores and not loaded onto the outer surfaces of Co^{II}-MOF particles.[25]

In the second step, CQDs@Co^{II}-MOF, regarded as the self-sacrificing template, was oxidized and pyrolyzed at 300 °C for 2 h in air. Excitedly, the solid tetrahedral arrays covering CoF have been changed to the hollow polyhedral arrays Co_3O_4@CQDs-CN HPAs (Figure 2c,d). Also, oxidation pyrolysis obviously expands the size of the building blocks (Figure 2a,c). More specifically, a closer observation (Figure 2e,f) clearly finds that the hollow polyhedra are composed of porous and uniform honeycomb-like nanosheet arrays with thin walls of ~60 nm thickness. The images of high-magnification FE-SEM (Figure 2f) and TEM (Figure 2g) show that numerous small NPs with ~20 nm diameter are uniformly imbedded on the matrix. The lattice spacing of 0.24 nm corresponds to the (311) plane of the spinel Co_3O_4,[26] while the crystal lattice fringes of 0.32 nm match well with the (002) crystallographic planes of graphitic carbon for CQDs (Figures 2h and S3).[27] The broad PL emission for Co_3O_4@CQDs-CN HPAs powders at 350−400 nm (λ_{ex} = 295 nm) confirms the presence of CQDs in the product (Figure S4). Elemental mapping (Figure 2i) from SEM−energy-dispersive X-ray spectroscopy (EDS) demonstrates uniform distribution of carbon, nitrogen, oxygen, cobalt, and phosphorus in the material. Moreover, powder XRD peaks located at 19.2°, 31.5°, 36.8°, and 44.8° correspond to the crystallographic planes (111), (220), (311), and (400) of the cubic spinel phase Co_3O_4, respectively (Figure 2b). The broad peaks centered at 24.2° and 42.8° agree well with those of graphitized carbon. The characteristic peak for CQDs at 26.2° is not found, which may explain the low content of CQDs.

To gain further insight into the effect of CQDs on Co_3O_4@CQDs-CN HPAs formation, we first examined the thermostability of CQDs. As shown in Figure S5, the first-stage weight loss (4.7%) occurs at 60−120 °C, which is assigned to the escape of adsorbed water molecules. A subsequent significant weight loss of 47.3%, which starts at 130 °C and ends at 315 °C, is assigned to the oxidation and decomposition of active moieties in CQDs during the process. From 316 to 400 °C, about 33.4% weight loss is attributed to the high carbonization of the CQD core.[28] This fact reflects that there are partial CQDs, resulting in the product after oxidation pyrolysis of

CQDs@Co^{II}-MOF at 300 °C. CQDs-free Co^{II}-MOF/CoF and its pyrolysis product Co_3O_4@CN/CoF were also monitored. FE-SEM images in Figure S6a clearly show that Co^{II}-MOFs on CoF are porous rectangular arrays instead of solid tetrahedral arrays of CQDs@Co^{II}-MOFs with smooth surfaces. The compacting role of the CQDs for Co^{II}-MOF may be the strong electrostatic interaction between CQDs with carboxyl (−COOH) and hydroxyl (−OH) groups and the Co^{II}-MOF framework. Compared with Co_3O_4@CQDs-CN HPAs with hollow and porous nanosheet arrays, Co^{II}-MOF-derived Co_3O_4@CN preserves the analogous solid rectangular backbone as its precursor (Figure S6b). Thus, we can conclude that CQDs in CQDs@Co^{II}-MOF play a crucial role in inflating and hollowing the compacted building blocks into hollow polyhedra because of their partial pyrolysis. Moreover, CQDs with excellent electron donors should be involved with air oxidation of the Co^{II} ion into Co_3O_4 nanocrystals and carbon hybrid nanosheet arrays.

X-ray photoelectron spectroscopy (XPS) measurements reveal that atomic fractions of C, N, O, Co, and P in Co_3O_4@CQDs-CN HPAs (Figure S7) are 32.24, 3.19, 34.26, 30.17, and 0.14%, respectively. Deconvolution C 1s peaks located at 284.8, 286.1, and 288.3 eV (Figure 3a) show the existence of sp^2-hybridized C in C═C, C−OH, and COOH, respectively. Another two at 284.2 and 285.3 eV represent C−C and C═N.[29] High-resolution O 1s peaks at 532.0 and 533.2 eV display C═O/O−C−OH and C−OH (Figure 3b). The O 1s spectrum at 531.2 eV is assigned to hydroxyl groups ($^{\bullet}$OH) resulting from surface defects.[16] In the Co 2p region (Figure 3c), four deconvoluted peaks for $2p_{3/2}/2p_{1/2}$ of Co^{3+} and Co^{2+} appear at 781.1/783.2 and 797.1/798.5 eV, while the corresponding shakeup satellite peaks are at 786.5/802.7 eV. The atomic ratio of Co^{3+}/Co^{2+} calculated by the fitted curve areas is ∼2:1, which matches well with the formula Co_3O_4 with the spinel crystal.[30] For the N 1s region (Figure 3d), graphitized nitrogen at 399.1 eV and pyrrolic nitrogen at 400.1 eV are the main nitrogen species, while the peak at 400.8 eV exhibits less pyridinic N.[31] These facts have manifested that the hollow polyhedral arrays of Co_3O_4@CQDs-CN HPAs are actually composed of uniform porous honeycomb-like nanosheets, in which small Co_3O_4 nanocrystals are highly dispersed on a CQDs-, pyrrolic nitrogen-, and pyridinic nitrogen-codoped sp^2-hybridized carbon matrix.

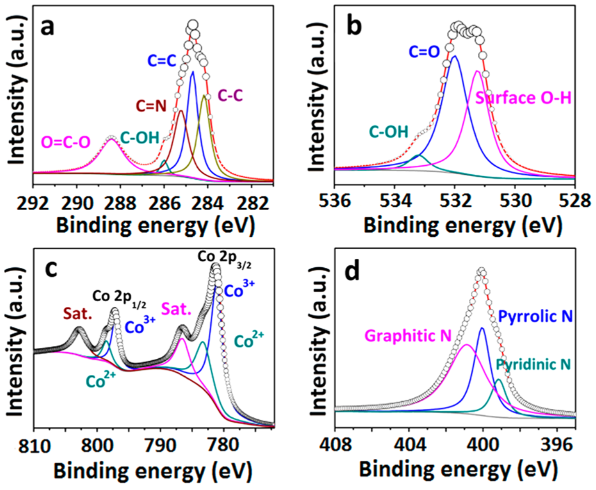

Figure 3. High-resolution XPS spectra of (a) C 1s, (b) O 1s, (c) Co 2p, and (d) N 1s for Co_3O_4@CQDs-CN HPAs.

The OER performances of self-supporting integrated materials directly as electrodes were investigated in 1.0 M KOH by linear sweep voltammetry (LSV) curves. The loading mass of each material on CoF was 1.7 ± 0.1 mg cm^{-2}. The LSV curves of the Co_3O_4@CQDs-CN/CoF materials with different CQD contents were initially explored. As shown as in Figure S8, their OER activities are obviously improved with increasing CQD concentrations in the precursor solution of CQDs@Co^{II}-MOF/CoF up to 11.2 mg mL^{-1}, above which the activities decrease. When CQD concentrations exceeds 16.8 mg mL^{-1}, the electrosynthesis of Co^{II}-MOF on NiF becomes very difficult because of growth of the CQDs-Co^{II} complex. Thus, the 11.2 mg mL^{-1} CQD concentration in the precursor solution was used in follow-up experiments. Figure S9 shows the LSV curves of the materials from oxidation pyrolysis of CQDs@Co^{II}-MOF/CoF at different temperatures. Clearly, the OER activities of the materials are highly dependent on the factor. The above-discussed CQDs-Co_3O_4@CN OHPA/CoF corresponding to 300 °C shows the lowest overpotential of 301 mV to drive the electric current density of 100 mA cm^{-2}, much smaller than those at 200 °C (392 mV), 400 °C (452 mV), and 500 °C (463 mV). We also compare the OER properties of the two materials, namely, the above-discussed CQDs-Co_3O_4@CN OHPA/CoF and another CQDs-Co_3O_4@CN/CoF, where CQDs-Co_3O_4@CN (Figure S10a) existing in the form of nanosheets is derived from oxidation pyrolysis of the rod-shaped CQDs@Co^{II}-MOF precursor (Figure S10b) at 300 °C for 2 h under air. The CQDs@Co^{II}-MOF precursor was prepared by a regular hydrothermal method. To achieve the electric current density of 100 mA cm^{-2}, the overpotential of CQDs-Co_3O_4@CN/CoF is 1.5 times that of CQDs-Co_3O_4@CN OHPA/CoF (446 mV compared to 301 mV; Figure S11). The result exhibits the important contribution of hollow polyhedral arrays composed of porous honeycomb-like nanosheets for the electrocatalytic performance.

Figure 4a clearly reveals that bare CoF shows negligible catalytic activity. In sharp contrast, the precursor CQDs@Co^{II}-MOF/CoF shows significantly enhanced OER activity over Co^{II}-MOF/CoF, implying a crucial role of CQDs for the OER performance. Particularly, Co_3O_4@CQDs-CN HPAs/CoF only needs an overpotential (η) of 301 mV to reach 100 mA cm^{-2}, achieving the highest OER activity among the materials, demonstrating that a hollow nanostructure with CQDs facilitates the OER performance. Also, this compares favorably to the catalytic behavior of RuO_2/CoF (η100 mA cm^{-2} = 316 mV). In addition, the presence of a phosphorus element in the present Co_3O_4@CQDs-CN HPAs/CoF has a negligible effect on its OER activity, which should be due to the low content of P in the material (0.14% from XPS analysis).

The Tafel slope of Co_3O_4@CQDs-CN HPAs/CoF (115 mV dec^{-1}) is greatly lower than those of CQDs-free Co_3O_4@CN/CoF (184 mV dec^{-1}) and the precursors CQDs@Co^{II}-MOF/CoF (170 mV dec^{-1}) and Co^{II}-MOF/CoF (187 mV dec^{-1}) but only slightly lower than that of RuO_2/CoF (127 mV dec^{-1}; Figure 4b). The result suggests that Co_3O_4@CQDs-CN HPAs/CoF possesses more rapid catalytic kinetics for OER than others do.[32]

Figure 4c displays the catalytic activity of Co_3O_4@CQDs-CN HPAs/CoF at 40 mA cm^{-2} being retrained for at least 25 h. Moreover, the LSV curves before and after continuous 1000 cyclic voltammetry (CV) scanning show negligible changes in

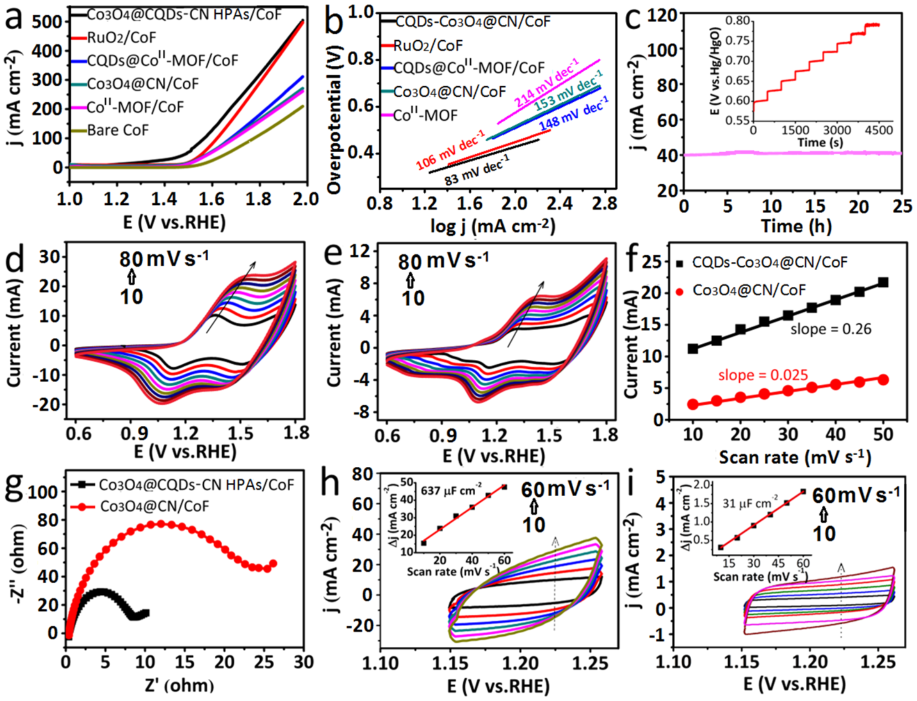

Figure 4. (a) LSV curves and (b) Tafel plots for Co_3O_4@CQDs-CN HPAs/CoF and its precursor CQDs@Co^{II}-MOF/CoF, Co_3O_4@CN/CoF and its precursor Co^{II}-MOF/CoF, RuO_2/CoF, and bare CoF. (c) Time-dependent current density for Co_3O_4@CQDs-CN HPAs/CoF at a 301 mV overpotential (inset: its multicurrent process). CVs of (d) Co_3O_4@CQDs-CN HPAs/CoF and (e) Co_3O_4@CN/CoF at different scan rates. (f) Linear relationship for the oxidation peak values and scan rates. (g) EIS comparison. (h and i) CVs for the nonfaradaic capacitance current interval (inset: linear dependence of the capacitive currents) at 0.30 V versus RHE on scan rates for (h) Co_3O_4@CQDs-CN HPAs/CoF and (i) Co_3O_4@CN/CoF. All were tested in 1.0 M KOH.

the current density (Figure S12). The inset in Figure 4c displays a multicurrent chronopotentiometric curve of Co_3O_4@CQDs-CN HPAs/CoF, with the current being increased from 50 to 275 mA cm^{-2} at an increment of 25 mA cm^{-2} per 500 s. Similar results remain in all steps, proving excellent mechanical properties, mass transportation, and conductivity for the Co_3O_4@CN HPAs/CoF electrode.[33] The SEM image of Co_3O_4@CN HPAs/CoF after continuous 1000 CV scanning shows negligible changes (Figure S13), further showing its robustness.

Parts d and e of Figure 4 reveal that the oxidation peak currents in the CV curves of Co_3O_4@CQDs-CN HPAs/CoF and Co_3O_4@CN/CoF are linearly dependent on the scan rates, suggesting a surface-controlled electrochemical process.[29,30] From slopes of 0.26 for Co_3O_4@CQDs-CN HPAs/CoF and 0.0025 for Co_3O_4@CN/CoF (Figure 4f), the number of active species (m) calculated for Co_3O_4@CQDs-CN HPAs/CoF is 2.8×10^{-7} mol, significantly higher than 2.7×10^{-9} mol for Co_3O_4@CN/CoF. The Nyquist plot in Figure 4g for Co_3O_4@CQDs-CN HPAs/CoF shows smaller charge-transfer resistance (7.5 Ω) at the overpotential of 300 mV than that of Co_3O_4@CN/CoF (25 Ω), indicating that the hierarchical structure can significantly enhance the charge-transfer rate.[13] Double-layer capacitance (C_{dl}) measured by the CV technique is closely related to the electrochemical active surface area (ECSA) of an electrode.[32] The C_{dl} value of 637 μF cm^{-2} for Co_3O_4@CQDs-CN HPAs/CoF is about 20 times larger than that for Co_3O_4@CN/CoF (31 μF cm^{-2}; Figure 4h,i), suggesting that Co_3O_4@CQDs-CN HPAs in hierarchical architecture owns significantly increased ECSA.

4. CONCLUSIONS

In summary, we successfully fabricate hollow polyhedral arrays Co_3O_4@CQDs-CN HPAs/CoF, composed of a Co_3O_4 nanocrystal ensemble on honeycomb-like carbon hybrid nanosheet arrays. The crucial roles of CQDs that hollow the polyhedra and form nanosheet arrays are proven. Significantly, the resulting hierarchical structure (i) can maximize utilization of the Co_3O_4 catalyst due to the high dispersion of Co_3O_4 nanocrystals, (ii) ensure sufficient highways for charge and mass storage and delivery because of the hollow hierarchical porous nanostructure and nanosheet arrays, (iii) offer enhanced catalyst activity and stability born of CQDs, nitrogen dopants, and a carbon matrix. This work opens a new route to preparing carbon-based metal oxide hollow nanoarrays with high catalytic activity for various energy conversions.

■ ASSOCIATED CONTENT

Ⓢ Supporting Information

The Supporting Information is available free of charge on the ACS Publications website at DOI: 10.1021/acs.inorgchem.8b03236.

> Materials used, electrochemical and structural characterizations, a table related to the present catalyst in comparison with MOF-derived and Co_3O_4 NPs-based OER electrocatalysts, and figures related to UV−vis and PL spectra, TEM and FE-SEM images, a XPS survey spectrum, and LSV and TG curves (PDF)

■ AUTHOR INFORMATION

Corresponding Authors

*E-mail: chm_kuangx@ujn.edu.cn (X.K.).

*E-mail: kuangr1985@foxmail.com (R.K.).
*E-mail: sdjndxwq@163.com (Q.W.).

ORCID

Yong Zhang: 0000-0002-5831-637X
Qin Wei: 0000-0002-3034-8046

Notes

The authors declare no competing financial interest.

ACKNOWLEDGMENTS

This work was supported by National Key Scientific Instrument, Equipment Development Project of China (Grant 21627809), and National Natural Science Foundation of China (Grants 21605058, 21575050, and 21375047).

REFERENCES

(1) Ma, M.; Ge, R.; Ji, X.; Ren, X.; Liu, Z.; Asiri, A. M.; Sun, X. Benzoate Anions-Intercalated Layered Nickel Hydroxide Nanobelts Array: An Earth-Abundant Electrocatalyst with Dreatly Enhanced Oxygen Evolution Activity. *ACS Sustainable Chem. Eng.* **2017**, *5*, 9625−9629.

(2) Reier, T.; Pawolek, Z.; Cherevko, S.; Bruns, M.; Jones, T.; Teschner, D.; Selve, S.; Bergmann, A.; Nong, H. N.; Schlögl, R.; Mayrhofer, K. J.; Strasser, P. Molecular Insight in Structure and Activity of Highly Efficient, Low-Ir Ir-Ni Oxide Catalysts for Electrochemical Water Splitting (OER). *J. Am. Chem. Soc.* **2015**, *137*, 13031−13040.

(3) Li, H.; Chen, S.; Zhang, Y.; Zhang, Q.; Jia, X.; Zhang, Q.; Gu, L.; Sun, X.; Song, L.; Wang, X. Systematic Design of Superaerophobic Nanotube-Array Electrode Comprised of Transition-Metal Sulfides for Overall Water Splitting. *Nat. Commun.* **2018**, *9*, 2452−2463.

(4) Anantharaj, S.; Reddy, P. N.; Kundu, S. Core-Oxidized Amorphous Cobalt Phosphide Nanostructures: An Advanced and Highly Efficient Oxygen Evolution Catalyst. *Inorg. Chem.* **2017**, *56*, 1742−1756.

(5) Men, Y.; Liu, X.; Yang, F.; Ke, F.; Cheng, G.; Luo, W. Carbon Encapsulated Hollow Co3O4 Composites Derived from Reduced Graphene Oxide Wrapped Metal-Organic Frameworks with Enhanced Lithium Storage and Water Oxidation Properties. *Inorg. Chem.* **2018**, *57*, 10649−10655.

(6) Zhu, Y. P.; Ma, T. Y.; Jaroniec, M.; Qiao, S. Z. Self-Templating Synthesis of Hollow Co Microtube Arrays for Highly Efficient Water Electrolysis. *Angew. Chem., Int. Ed.* **2017**, *56*, 1324−1328.

(7) Yuan, C.; Wu, H. B.; Xie, Y.; Lou, X. W. Mixed Transition-Metal Oxides: Design, Synthesis, and Energy-Related Applications. *Angew. Chem., Int. Ed.* **2014**, *53*, 1488−1504.

(8) Qin, Y.; Zhang, F.; Chen, Y.; Zhou, Y.; Li, J.; Zhu, A.; Luo, Y.; Tian, Y.; Yang, J. Hierarchically Porous Cu Hollow Spheres Fabricated via A One-Pot Template-Free Method for High-Performance Gas Sensors. *J. Phys. Chem. C* **2012**, *116*, 11994−12000.

(9) Benzigar, M. R.; Talapaneni, S. N.; Joseph, S.; Ramadass, K.; Singh, G.; Scaranto, J.; Ravon, U.; Al-Bahily, K.; Vinu, A. Recent Advances in Functionalized Micro and Mesoporous Carbon Materials: Synthesis and Applications. *Chem. Soc. Rev.* **2018**, *47*, 2680−2721.

(10) Hu, X.; Wang, C.; Li, J.; Luo, R.; Liu, C.; Sun, X.; Shen, J.; Han, W.; Wang, L. Metal-Organic Framework-Derived Hollow Carbon Nanocubes for Fast Solid-Phase Microextraction of Polycyclic Aromatic Hydrocarbons. *ACS Appl. Mater. Interfaces* **2018**, *10*, 15051−15057.

(11) Tao, H.; Yan, C.; Robertson, A. W.; Gao, Y.; Ding, J.; Zhang, Y.; Ma, T.; Sun, Z. N-Doping of Graphene Oxide at Low Temperature for The Oxygen Reduction Reaction. *Chem. Commun.* **2017**, *53*, 873−876.

(12) Clancy, A. J.; Bayazit, M. K.; Hodge, S. A.; Skipper, N. T.; Howard, C. A.; Shaffer, M. S. P. Charged Carbon Nanomaterials: Redox Chemistries Fullerenes, Carbon Nanotubes, and Graphenes. *Chem. Rev.* **2018**, *118*, 7363−7408.

(13) Wang, X.; Tian, W.; Zhai, T. Y.; Zhi, C. Y.; Bando, Y.; Golberg, D. Cobalt (II,III) Oxide Hollow Structures: Fabrication, Properties and Applications. *J. Mater. Chem.* **2012**, *22*, 23310−23326.

(14) Wang, G. H.; Hilgert, J.; Richter, F. H.; Wang, F.; Bongard, H. J.; Spliethoff, B.; Weidenthaler, C.; Schüth, F. Platinum-Cobalt Bimetallic Nanoparticles in Hollow Carbon Nanospheres for Hydrogenolysis of 5-Hydroxymethylfurfural. *Nat. Mater.* **2014**, *13*, 293−300.

(15) Ying, J.; Jiang, G.; Paul Cano, Z.; Han, L.; Yang, X. Y.; Chen, Z. Nitrogen-Doped Hollow Porous Carbon Polyhedrons Embedded with Highly Dispersed Pt Nanoparticles as A Highly Efficient and Stable Hydrogen Evolution Electrocatalyst. *Nano Energy* **2017**, *40*, 88−94.

(16) Kuang, X.; Luo, Y. C.; Kuang, R.; Wang, Z. L.; Sun, X.; Zhang, Y.; Wei, Q. Metal Organic Framework Nanofibers Derived Co$_3$O$_4$-Doped Carbon-Nitrogen Nanosheet Arrays for High Efficiency Electrocatalytic Oxygen Evolution. *Carbon* **2018**, *137*, 433−441.

(17) Kaneti, Y. V.; Tang, J.; Salunkhe, R. R.; Jiang, X.; Yu, A.; Wu, K. C.-W.; Yamauchi, Y. Nano-Architectured Design of Porous Materials and Nanocomposites from Metal-Organic Frameworks. *Adv. Mater.* **2017**, *29*, 1604898−1604937.

(18) Stassen, I.; Burtch, N.; Talin, A.; Falcaro, P.; Allendorf, M.; Ameloot, R. An Updated Roadmap for The Integration of Metal-Organic Frameworks with Electronic Devices and Chemical Sensors. *Chem. Soc. Rev.* **2017**, *46*, 3185−3241.

(19) Guan, B. Y.; Yu, X. Y.; Wu, H. B.; Lou, X. W. D. Complex Nanostructures from Materials Based on Metal-Organic Frameworks for Electrochemical Energy Storage and Conversion. *Adv. Mater.* **2017**, *29*, 1703614−1703623.

(20) Zhu, C.; Fu, Y.; Liu, C.; Liu, Y.; Hu, L.; Liu, J.; Bello, I.; Li, H.; Liu, N.; Guo, S.; Huang, H.; Lifshitz, Y.; Lee, S. T.; Kang, Z. Carbon Dots as Fillers Inducing Healing/Self-Healing and Anticorrosion Properties in Polymers. *Adv. Mater.* **2017**, *29*, 1701399−1701405.

(21) Wei, G.; He, J.; Zhang, W.; Zhao, X.; Qiu, S.; An, C. Rational Design of Co(II) Dominant and Oxygen Vacancy Defective CuCo$_2$O$_4$@CQDs Hollow Spheres for Enhanced Overall Water Splitting and Supercapacitor Performance. *Inorg. Chem.* **2018**, *57*, 7380−7389.

(22) Wang, H.; Getzschmann, J.; Senkovska, I.; Kaskel, S. Structural Transformation and High Pressure Methane Adsorption of Co$_2$(1,4-bdc)$_2$dabco. *Microporous Mesoporous Mater.* **2008**, *116*, 653−657.

(23) Gu, Z. G.; Li, D. J.; Zheng, C.; Kang, Y.; Wöll, C.; Zhang, J. MOF-Templated Synthesis of Ultrasmall Photoluminescent Carbon-Nanodot Arrays for Optical Applications. *Angew. Chem., Int. Ed.* **2017**, *56*, 6853−6858.

(24) Yang, Z. C.; Wang, M.; Yong, A. M.; Wong, S. Y.; Zhang, X. H.; Tan, H.; Chang, A. Y.; Li, X.; Wang, J. Intrinsically Fluorescent Carbon Dots with Tunable Emission Derived from Hydrothermal Treatment of Glucose in The Presence of Monopotassium Phosphate. *Chem. Commun.* **2011**, *47*, 11615−11617.

(25) Hou, J.; Yan, J.; Zhao, Q.; Li, Y.; Ding, H.; Ding, L. A Novel One-Pot Route for Large-Scale Preparation of Highly Photoluminescent Carbon Quantum Dots Powders. *Nanoscale* **2013**, *5*, 9558−9561.

(26) Suryanto, B. H. R.; Lu, X. Y.; Zhao, C. Layer-by-Layer Assembly of Transparent Amorphous Co$_3$O$_4$ Nanoparticles/Graphene Composite Electrodes for Sustained Oxygen Evolution Reaction. *J. Mater. Chem. A* **2013**, *1*, 12726−12731.

(27) Miner, E. M.; Fukushima, T.; Sheberla, D.; Sun, L.; Surendranath, Y.; Dincă, M. Electrochemical Oxygen Reduction Catalysed by Ni$_3$(Hexaiminotriphenylene)$_2$. *Nat. Commun.* **2016**, *7*, 10942−10948.

(28) Li, F.; Li, Y.; Yang, X.; Han, X.; Jiao, Y.; Wei, T.; Yang, D.; Xu, H.; Nie, G. Highly Fluorescent Chiral N-S-Doped Carbon Dots from Cysteine Affect Cellular Energy Metabolism. *Angew. Chem., Int. Ed.* **2018**, *57*, 2377−2382.

(29) Xu, C.; Wang, X.; Zhu, J.; Yang, X.; Lu, L. Deposition of Co$_3$O$_4$ Nanoparticles onto Exfoliated Graphite Oxide Sheets. *J. Mater. Chem.* **2008**, *18*, 5625−5629.

(30) Li, H. F.; Zhao, Q. H.; Xie, M. J.; Qian, F. H. Synthesis, Crystal Structure and Luminescent Properties of a Coordination Polymer of Cyanuric Acid. *Chin J. Inorg. Chem.* **2013**, *29*, 355−359.

(31) Ji, X. Q.; Zhang, R.; Shi, X. F.; Asiri, A. M.; Zheng, B. Z.; Sun, X. P. Fabrication of Hierarchical Cop Nanosheet@Microwire Array via Space-Confined Phosphidation toward High-Efficiency Water Oxidation Electrocatalysis under Alkaline Conditions. *Nanoscale* **2018**, *10*, 7941−7945.

(32) Xie, M.; Xiong, X.; Yang, L.; Shi, X.; Asiri, A. M.; Sun, X. An $Fe(TCNQ)_2$ Nanowire Array on Fe Foil: An Efficient Non-Noble-Metal Catalyst for The Oxygen Evolution Reaction in Alkaline Media. *Chem. Commun.* **2018**, *54*, 2300−2303.

(33) Wu, D.; Wei, Y.; Ren, X.; Ji, X.; Liu, Y.; Guo, X.; Liu, Z.; Asiri, A. M.; Wei, Q.; Sun, X. $Co(OH)_2$ Nanoparticle-Encapsulating Conductive Nanowires Array: Room-Temperature Electrochemical Preparation for High-Performance Water Oxidation Electrocatalysis. *Adv. Mater.* **2018**, *30*, 1705366−1705372.

DOI: 10.1021/acs.inorgchem.8b03236
Inorg. Chem. XXXX, XXX, XXX−XXX